

Theoretical and experimental study of electromagnetic forces induced in one-dimensional photonic crystals

J. E. Lugo¹, Rafael Doti¹, Jocelyn Faubert¹, Noemi Sanchez^{1,2}, Javier Sanchez², Martha A. Palomino³, M. Beatriz de la Mora⁴ and J. Antonio del Rio⁵

¹Visual Psychophysics and Perception Laboratory, School of Optometry, University of Montreal, C.P. 6128 succ. Centre Ville, Montreal, Quebec, Canada H3C3J7, ² Instituto Nacional de Astrofísica, Óptica y Electrónica, Calle Luis Enrique Erro #1. Tonantzintla, Puebla, México. 72000, ³ Facultad de Ciencias Físico Matemáticas, Benemérita Universidad Autónoma de Puebla, Av. San Claudio y Río Verde, Col. San Manuel, Puebla, México, 72570, ⁴ Instituto de Física, Departamento de Estado Solido, Universidad Nacional Autónoma de México, México, D. F., México, 04510, ⁵ Centro de Investigación en Energía, Universidad Nacional Autónoma de México, Temixco 62580, Morelos, Mexico

We studied theoretically and experimentally the induction of electromagnetic forces in one-dimensional photonic crystals with localized defects when light impinges transversally to the defect layer. The theoretical calculations indicate that the electromagnetic forces increases at a certain frequency that coincide with a defect photonic state. The photonic structure consists of a microcavity like structure formed of two one-dimensional photonic crystals made of free-standing porous silicon, separated by variable air gap and the working wavelength is 633 nm. The force generation is made evident by driving a laser light by means of a chopper; the light hits the photonic structure and induces a vibration and the vibration is characterized by using a very sensitive vibrometer.

Keywords: Electromagnetic force, porous silicon, light propagation, photonic crystals, defect states.

*eduardo.lugo@gmail.com; phone 514-3436111 ext. 1685.

1. INTRODUCTION

The concept of radiation pressure has been used in the past for manipulating micro-objects [1]. For example, optical tweezers are used to levitate viruses, bacteria, cells, and sub cellular organisms, etc. [2]. The fast development of electromagnetic wave driven micro motors has motivated several research groups to investigate novel working principles for such micro motors [3], but there is a main obstacle, normally the radiation pressure is too small for this kind of applications [4]. Nonetheless some resonance principles can be used to increase the force significantly. For instance, a waveguide made of lossless dielectric blocks, where the direction of the force exerted on the dielectric is parallel to the waveguide axis [5, 6]. A second approach is a Bragg waveguide, based on a Fabry-Perot cavity in which the peak of the force only appears at the structures' resonant frequencies and the force is normal to the waveguide wall [7]. However in this design the force tends to separate the two mirrors that form the Fabry-Perot cavity, having as a consequence a dramatic reduction of the force [4]. A third approach can use a one-dimensional photonic crystal with structural defects, where a localized mode results in strong electromagnetic fields around the position of the defect. Thus, the strong fields enhance the tangential and normal force on a lossy dielectric layer [4]. This work is organized as follows: in the first section we describe briefly the theory to induce an electromagnetic force in the photonic structure. Next, we present the experimental details to fabricate the photonic structure and how to measure the structure movement, velocity, and acceleration. Then, we present and discuss the results where we compare the experimental force with the theoretical one. Finally we wrap up the work by giving some conclusions.

2. THEORY

Consider the structure depicted on figure 1. Let us assume that light impinges at normal incidence with the electric field polarized in the y-direction and with magnitude:

$$E_y = E(x)e^{j(\omega t - \beta z)}, \quad (1)$$

where

$$E(x) = \begin{cases} A_0 e^{-jk_0(x-x_0)} + B_0 e^{jk_0(x-x_0)} & x < x_0 \\ A_l e^{-jk_l(x-x_l)} + B_l e^{jk_l(x-x_l)} & x_{l-1} < x < x_l \\ A_s e^{-jk_s(x-x_N)} + B_s e^{jk_s(x-x_N)} & x_N < x \end{cases}, \quad (2)$$

where all A_i 's and B_i 's are the complex amplitudes of the electric field in each region of the structure plus the air (0 label) and the substrate (s label) and the k_i 's are the wavevectors at the different regions on the structure in the x-direction and β is the wavevector in the z-direction. The k_i 's are given by $\omega n_i/c$, where n_i is the refractive index of region i and c is the speed of light. By using a similar formalism as presented in [4, 8] it is possible to show that for lossless dielectrics the surface force density only exist in the x-direction and is given by:

$$\langle F_x \rangle_T = \sum_{l=1}^N \frac{\epsilon_0}{4} \left[\left(\frac{n_{l-1}}{n_l} \right)^4 - 1 \right] \left[|A_l|^2 + |B_l|^2 + 2|A_l||B_l| \cos(2k_l d_l + \varphi_{A_l} - \varphi_{B_l}) \right] + \sum_{l=1}^N \frac{\epsilon_0}{2} \left[(n_l)^2 - 1 \right] |A_l||B_l| \begin{bmatrix} \cos(\varphi_{A_l} - \varphi_{B_l}) - \cos(2k_l d_l + \varphi_{A_l} - \varphi_{B_l}) \end{bmatrix} \quad (3)$$

where ϵ_0 is the vacuum permittivity. The complex amplitudes A_i 's and B_i 's and their phases φ_i can be calculated by using the well known transfer matrix method [9].

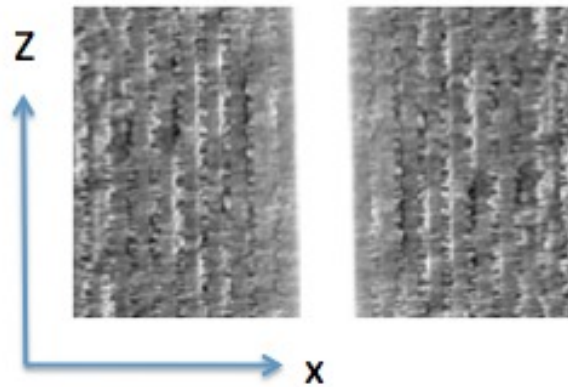


Figure 1. 1D PC structure. SEM picture showing the layers and a defect region. The light impinges at the left interface (air) cross the photonic structure and exits at the right interface on the substrate (glass)

3. EXPERIMENTAL

Porous silicon (Psi) photonic crystals (Fig. 1) were prepared by electrochemical anodization of crystalline silicon (c-Si)[10]. Porous silicon was fabricated by wet electrochemical etching of highly boron-doped c-Si substrates with orientation (100) and electrical resistivity of 0.001–0.005 Ohm-cm (room temperature=25°C, humidity=30%). On one side of the c-Si wafer, an aluminum film was deposited and then heated at 550°C during 15 minutes in nitrogen atmosphere to produce a good electrical contact. In order to have flat interfaces, an aqueous electrolyte composed of HF/ethanol/glycerol was used to anodize the silicon substrate. It is well known that the Psi refractive index increases by decreasing the electrical current applied during the electrochemical etching. However, reducing the porosity too much might stop the electrolyte flow through the porous and limit the subsequent high porosity layer that makes the contrast. One way to allow the electrolyte to flow is by increasing the ethanol fraction in the solution. For this reason, an electrolyte composition of 3:7:1 was used. In addition, the HF concentration was maintained constant during the etching process using a peristaltic pump to circulate the electrolyte within the Teflon™ cell. Anodization begins when a constant current is applied between the c-Si wafer and the electrolyte by means of an electronic circuit controlling the anodization process. To produce the multilayers, current density applied during the electrochemical dissolution was alternated from 3 mA/cm² (layer a) to 40 mA/cm² (layer b) and 10 periods (20 layers) were made. The current density conditions give layers with porosities of 65% and 88% respectively. In order to obtain a free standing Psi photonic crystals, at the end of the formation process an anodic electropolishing current pulse (500 mA/cm² for 2s) was applied to detach the structure. Psi samples were partially oxidized at 350 °C for 10 minutes. The best refractive index values we found that fit the experimental photonic bandgap structure (not shown) are $n_1 = 1.1$ and $n_2 = 2$. Scanning electron microscopy (SEM) was used to measure the films thicknesses, which were $d_1 = 326 \pm 11$ nm and $d_2 = 435 \pm 11$ nm.

For building the vibrating device, two pieces of these samples have to be placed in a mirror like symmetry and letting a gap space between them. As the Psi foil is an elastic and very fragile material, it is difficult to manipulate, because it is susceptible to present static electric charge. These characteristics, added to the poor mechanical resistance of the multilayer structure, impose the concept of building a device as simple as possible. Another problem is that the Psi foil is not a flat membrane. As explained before, after being generated the multilayer porous structure and separated from the c-Si. The resulting membrane accumulates mechanical stress that deforms slightly the original flat structure. As the foils are not completely flat, it is a problem because the “defect” condition requires that both pieces of foil are parallel. So, we tried to reach the right geometric condition in two configurations. In the first, we fixed two samples of Psi (one over the other) by means of the adhesive tape applied to one end of both specimens over a glass substrate. This means the same end for both. In this case the device has a cross section similar to a “V”, where ideally the air gap is linearly increased along the Psi foils as shown in figure 2.

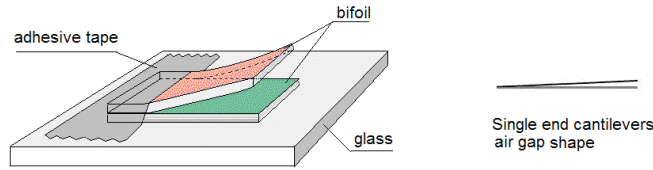


Figure 2. Schematic representation of the porous silicon bifoil device. In this case the device presents single end Psi cantilevers.

In this case the defect condition must be verified for only a thin ideal band as shown in figure 3. As the foils are not flat, the defect condition really is verified for a partial area of the ideal band.

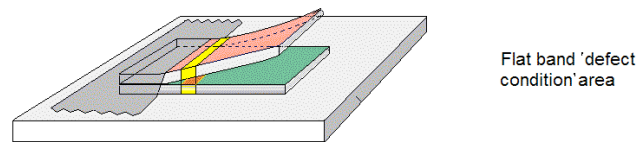


Figure 3. For the single end cantilevers geometry the defect condition must be verified for only a thin ideal band.

The second configuration consists in fixing each foil with the adhesive tape but this time from opposite ends. Figure 4 shows both foils overlapped over the glass substrate. The inconvenient of this configuration is that the 'defect' condition could be difficult to achieve. Nevertheless, the advantages of this configuration are: both samples became more flat because the equilibrium forces for both pieces of foil make them react one against each other, and the 'defect' condition could be verified for a larger surface area. Note that this surface area is not the whole available surface area of a foil. This is shown in figure 5, where we can see a representation on how the active surface areas are distributed over the foils. Even, they could be different from one cycle to another (dangling defect condition). The experimental results confirmed that both configurations worked, but the second one was more effective and stable. Once we gain some experience in manipulating the foil, as much as in mounting the device, we produce a dozen prototypes with small differences in the pieces shape, and/or in the overlapped portion of Psi foils. The device showed a great robustness for all the prototypes tested.

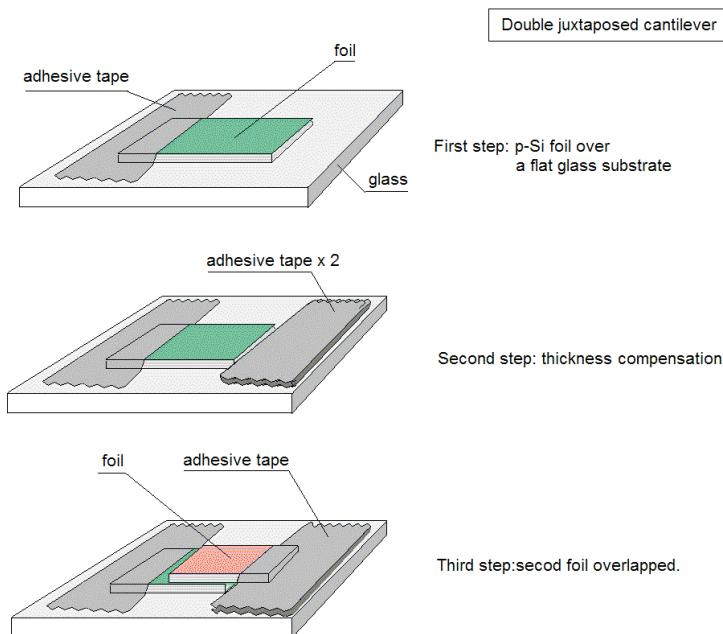


Figure 4. Here, the foils are overlapped over the glass substrate but the cantilevers are juxtaposed from opposite ends.

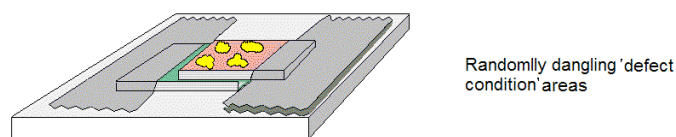


Figure 5. In the case of the juxtaposed cantilevers, the 'defect' condition could be verified for larger areas that may be divided in several small portions distributed over the foils. Even, they could differ from one cycle to another (dangling defect condition areas)

3.1 Methods and Materials:

The general set up and lay out is shown in figure 6 . There we found:

- 1) The Psi photonic structure device mounted on a glass substrate (bifoil device).
- 2) A precision rotation stage (DADEAL Inc.) with an X-Y micrometric positioning table (Parker).
- 3) A circular variable metallic neutral density filters (turning light attenuator). Newport model: 50G02AV.2, diameter 127 mm.
- 4) Infra Red band pass filter (Techspec Edmund cut-off 650 nm)
- 5) He-Ne Laser, power 13 mw, waveleght: 633 nm, beam diameter 2.58 mm (REO type LHRP 0501)

- 6) An electromagnetic beam chopper (MFE model R4077 open loop galvanometer 90Hz)
- 7) A near infrared (wavelength: 780 nm, power: 15 mw) Laser vibration meter (VibroMet 500V)
- 8) A light detector (Tektronix Inc., model J6505, red candles)
- 9) A control computer
- 10) Oscilloscope (Agilent U 1604A, 40 MHz)
- 11) A signal generator (Topward Electric Instruments Ltd., model 8120)
- 12) A laser beam polarizer (Techspec Edmund 400-700nm)

The experiment consisted in pumping optically the photonic structure (1) with a Laser beam (5) modulated by the beam chopper (6), while measuring the instant position of the external Psi foil by means of the vibration meter (7). The signal generator (11) provided the electrical excitatory signal to the chopper. We tested the classic: sinusoidal, saw-tooth, and square waveforms. As the chopper was based on a linear electromagnetic rotating transducer, the different electric waveforms used as excitation signals gave the corresponding light intensity shapes in the time domain. These shapes are the result of the transducer oscillating rotation (open loop galvanometer), moving a triangular steel blade used to interrupt the laser beam. The light detector (8) was used to record the resulting signal of the excitatory light intensity. The vibration meter sends a near infrared Laser beam to the target (external foil of the the photonic structure) its reflection is introduced back into the vibration meter where the movement amplitude, velocity and its Fourier spectrum (amplitude and frequency), and the aceleration are evaluated. The testing set-up sequence for the photonic structure is:

- Alignment of the vibration-meter laser at 20 degrees from the normal perpendicular to the photonic structure. This is a near infrared 15 mw laser.
- Aiming the measurement laser spot close to center of the photonic structure surface area.
- Alignment of the pumping a 13 mw red He-Ne laser, spotting the center of the photonic structure surface area.
- Starting the signal generator with a low voltage (150 mV peak) sinusoidal signal of about 5 Hz. We wish the amplitude of the chopper blade (triangular shape) movement a little bit larger than the pumping laser beam diameter (3 mm) to ensure both: the maximum 10 miliwatts excitation, and the zero (black) light condition. The generator we used permitted the addition of a DC component to the electric chopper signal. This helped aligning the central position of the toggle blade movement with the center of the laser beam.

Once the optical pumping begins, the photonic structure starts moving. The structure sometimes behaved with some degree of hysteresis due to the phase shift between the elastic recovery of the device, and the chopper movement (or the light pumping). In these cases we tried to improve the set up alignment while the experiment was running for both, the excitation laser, and the vibration-meter laser. In addition we vary de signal DC component for the chopper (that is, changing the phase shifting). The reference for this task was the detected movement speed signal intensity present on the computer monitor. We remark that the signal processing software execution introduces a delay between the movement fact and the movement speed dynamic graphic on the monitor. This delay is not significant for improving the set up alignment. The experiment showed to be sensitive to the vibration-meter laser alignment but it showed to be very robust in reference to the excitation laser alignment, instead.

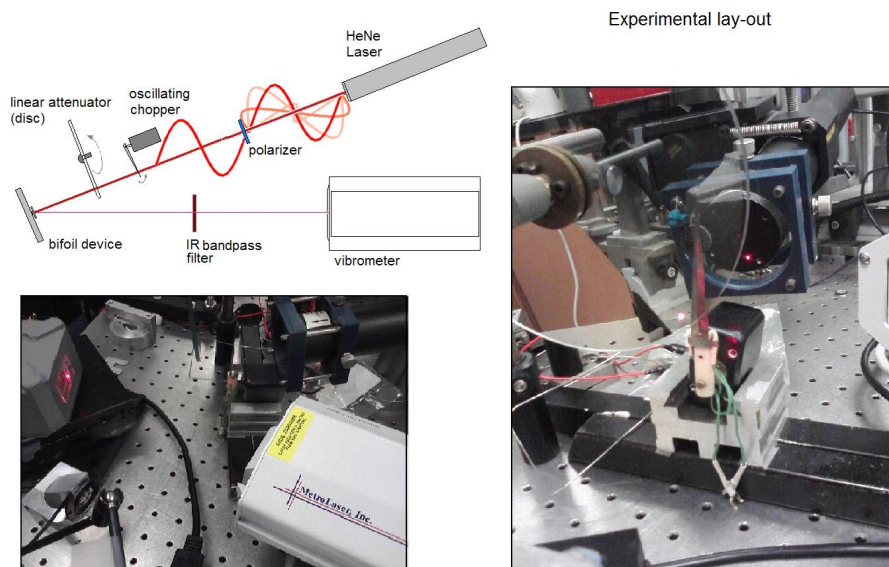


Figure 6. Experiment lay-out. Showing the different devices mentioned in the above description.

We explore different chopper excitation signals with frequencies between 5 Hz and 40 Hz, for sinusoidal, triangular, and square electric waveforms. To ensure the optimal blade movement alignment we simply varied the DC level on the signal generator while looking for bigger signal amplitude on the screen.

The photonic structure was tested and maintained at 23 Celsius degrees, and 30 % relative humidity environmental conditions, as the Psi foil is hygroscopic.

All the structures showed to be reliable and repetitive along the test. Those prototypes with larger dimensions (for instance: 4mm x 6mm) presented higher crack sensitivity. Their lifetime was of few hours when pumped between 5 Hz and 25 Hz with foil movement amplitude around 5 microns. The smaller ones (2.5 mm x 3.5 mm) showed to be more crack resistant even with movement amplitudes from 8 to 10 microns, and their lifetime surpassed 20 hours. In our experiment the electric forces (induced by the optical pumping at frequencies from 5 up to 40 Hz) deform the whole porous multilayer structure creating elastic reactions. However, the specific required condition that makes possible the emergence of the electric force between both foils (called “defect”) make evident that the different porous structure can bear the associated deformations without collapsing or cracking. If we analyze a whole vibration cycle we find that when the pumping light initiates the device deformation the structure immediately leaves the “defect” condition. Clearly the electric force momentum makes the Psi foil to continue deforming even after that momentum extinguishes. When the accumulated elastic reaction reaches the equilibrium point, then the movement stops. After that, the elastic force may return the foil to the original position. To continue vibrating the whole device after being deformed by the electric forces has to return exactly to the same or other “defect” condition. However, it doesn’t mean that the “defect” is located always in the same portion of the overlapped area. For each movement the condition could be achieved in a different region of the overlapped area under the pumping light spot, and not necessarily all the times in the same region on the structure. This creates a movement shape drift that we verified in the measured signals records. Nevertheless, for the devices we tested at specific frequencies as 4 Hz, 8Hz, 12Hz, 16Hz, and 20Hz, we verified a very stable performance. This is for the devices having a smaller active area. Finally, once one of the foils suffered a crack (generally the external one) the movement stopped. Sometimes a piece of a foil was completely torn and the device destroyed.

3. RESULTS

Figure 7 shows a typical vibration measurement output. The chopper driven electrical signal was sinusoidal and the optical pumping signal had square waveform shape with a duty cycle of 50% approximately, frequency of 12 Hz and 13 mW of power. In figure 7 we can see that the photonic structure oscillates mainly at a frequency of 11 Hz with amplitude of 30 microns approximately and an acceleration of 0.14 m/s^2 . We can estimate the net mechanical force induced on the structure by multiplying the mass of one foil of the structure and the acceleration. The surface area of this photonic device was 3 mm^2 and the total thickness of a photonic crystal structure is $10 \times (761 \times 10^{-9}) \text{ m}^2$ this give us a volume of $2.283 \times 10^{-11} \text{ m}^3$. The volumetric density of each layer is the product of $(1-P) \times 2330 \text{ kg/m}^3$, where P means porosity. The value of 2330 corresponds to the volumetric density of c-Si. Since the whole photonic structure contains both porous layers we can take a weight average of both densities where the weights correspond to each thickness. The final result is 586 kg/m^3 . Multiplying the volume times the effective volumetric density give us the mass estimation which has a value of $1.33784 \times 10^{-8} \text{ Kg}$. Finally the mechanical force would be $1.87297 \times 10^{-9} \text{ N}$.

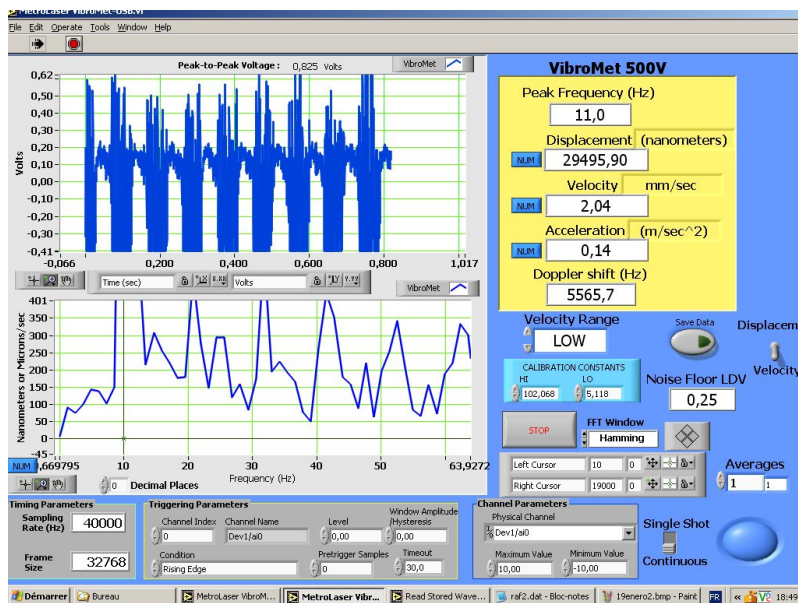


Figure 7. Shows a typical vibration measurement, where we can see the amplitude of the movement, the velocity, the acceleration and the velocity Fourier spectrum.

Now let us use equation 3 to calculate the electromagnetic force induced in the structure. We know that the force is going to depend on the defect length and the light power. For instance in figure 8 we can see the force profiles for different defect lengths and light power. Clearly there is a resonance at a defect length of $7 \times (n_1 d_1 + n_2 d_2)$ for all light powers. For 13 mW the lowest force magnitude is found at $10 \times (n_1 d_1 + n_2 d_2)$ with a value of 10 nN, which is approximately five times bigger than the experimental force we found. We can explain this difference by using a simple model where the mechanical acceleration can be approximated as $a = -\omega_0^2 x - (\beta / m) \dot{x} + \langle F_x \rangle_T / m$, where x and \dot{x} are the vibration amplitude and its velocity respectively, ω_0 is the natural frequency of the structure, β is a damping factor and m is the mass. We can see that we have to subtract from the electromagnetic force a harmonic force at a viscous damping force meaning that more than 80% of the work done by the electromagnetic force is lost due to viscosity effects between the air and the Psi moving foil. This would be problematic when thinking on practical applications. A point that will be discussed in the future because it is beyond the scope of the present work. Figure 9 shows that the behavior of the electromagnetic force, at resonance, against different power levels is a linear relationship.

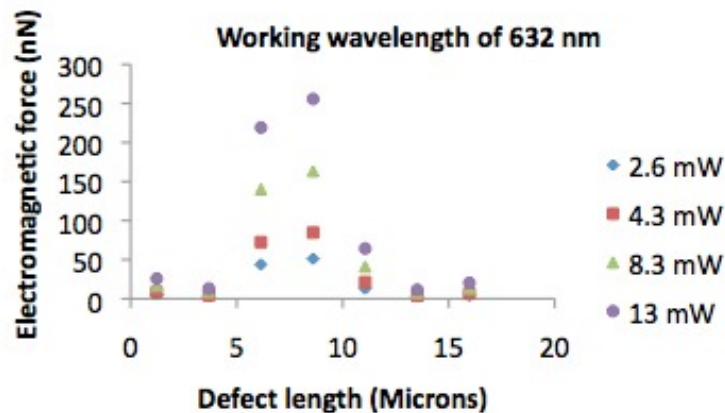


Figure 8. Electromagnetic force profile for different optical power levels and defect lengths.

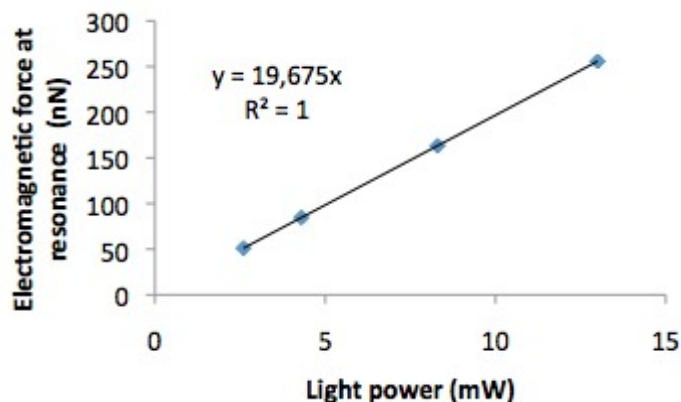


Figure 9. Theoretical linear relationship between the electromagnetic force and the light power.

4. CONCLUSIONS

We have shown theoretically and experimentally that it is possible to induce electromagnetic forces in a one-dimensional photonic crystal with defects by using a laser beam. This force is maximum at resonance and for the structure we used with maximum light power it would be of the order of 256 nN. However, the minimum force under the same power conditions should be of the order of 10 nN. Experimentally we measured a force of the order of 2 nN. This implies the existence of a huge lost energy due to a viscous damping effect. Although the losses, this force is 20 times bigger than the typical force of 100 pN produced by optical tweezers. From a practical point of view there are at least two photonic applications where this kind of principle would be beneficial. The first is a mechanically tunable photonic crystal that uses the concept of applying a mechanical force through a MEMS device to achieve dynamic tunability of the photonic band structure [11]. The second application is a mechanically tunable detector interface that uses a Psi layer integrated with a MEMS structure[12]. When a voltage is applied, the MEMS structure bends the Psi layer at different angles. If a laser beam hits the Psi surface the reflected beam can be spatially tune and select different detectors. If we use the principle of force generation we have presented here the MEMS device in both applications could be replaced to create devices activated only with light.

ACKNOWLEDGMENTS

This work was supported by the NSERC-Essilor Research Chair and an NSERC operating grant.

REFERENCES

1. Dholakia, K., Spalding, G., MacDonald, M., "Optical tweezers: the next generation," *Physics World*, 31-35 (2002).
2. Ashkin, A., Dziedzic, J.M., "Optical trapping and manipulation of viruses and bacteria," *Science* 235(4795), 1517-1520 (1987).
3. Higurashi, E., O. Ohguchi, T. Tamamura, H. Ukita, and R. Sawada, "Optically induced rotation of dissymmetrically shaped fluorinated polyimide micro-objects in optical traps," *J. Appl. Phys.* 82(6), 2773-2779 (1997).
4. Li, J. M., Shan, G. J., "Enhancement of electromagnetic force by localized fields in one-dimensional photonic crystal," *Progress In Electromagnetics Research M* 10, 59-70 (2009).
5. Gomez-Medina, R., San Jose, P., Garcia-Marin, A., Lester, M., Nieto-Vesperinas, M., Saenz, J. J., "Resonant radiation pressure on neutral particles in a waveguide," *Phys. Rev. Lett.* 86(19), 4275-4277 (2001).
6. Mizrahi, A., "Torque and longitudinal force exerted by eigenmodes on circular waveguides," *Phys. Rev. A* 78, 023802 (2008).
7. Povinelli, M.L., Ibanescu, M., Johnson, S. G., Joannopoulos, J. D., "Slow-light enhancement of radiation pressure in an omnidirectional-reflector waveguide," *Appl. Phys. Lett.* 85, 1466 (2004).
8. Mizrahi, A., Schachter L., "Electromagnetic forces on the dielectric layers of the planar optical Bragg acceleration structure," *Phys. Rev. E* 74, 036504 (2006).
9. Pochi, Y., [Optical waves in layered media], John Wiley & Sons, Inc., 102-141 (1988).
10. Nava R., de la Mora, M.B., Taguena-Martinez, J., del Rio, J.A., "Refractive index contrast in porous silicon multilayers," *Phys Status Solidi C*, 6, 1721 (2009).
11. Park, W., Lee, J.B., "Mechanically Tunable Photonic Crystals," *Optics and Photonics News*, 20(11), 41-45 (2009).
12. Song, D., Tokranova, N., Gracias, A., Castracane, J., "New approaches for chip-to-chip interconnects: integrating porous silicon with MOEMS," *J. Micro/Nanolith. MEMS MOEMS* 7(2), 021013 (2008).